Spatial distribution of recombination centers in GaAs:Te: Effects of the doping level

A. Castaldini, A. Cavallini, and B. Fraboni
Department of Physics, University of Bologna, I-40136 Bologna, Italy

B. Mendez and J. Piqueras
Departamento Física de Materiales, Facultad de Físicas, Universidad Complutense, 28040 Madrid, Spain

(Received 13 September 1993; accepted for publication 13 March 1994)

The distribution in liquid-encapsulated-Czochralski (LEC) GaAs:Te wafers of point and complex defects has been investigated together with their influence on the minority-carrier diffusion length L. Three wafers with different Te-doping concentration (2.2×10^{17}, 4.5×10^{17}, and 1.5×10^{18} cm^{-3}) have been studied by means of the electron-beam-induced-current (EBIC) mode of scanning electron microscopy and of the surface photovoltage (SPV) method. The morphology and electrical activity of the defects observed across each wafer have been correlated to the formation and distribution of deep electronic levels, which are significantly affected by the tellurium concentration. The diffusion length has been found to be mainly controlled by deep levels associated with dislocations. EBIC localized measurements of L and of the net ionized free-carrier concentration provide evidence for the influence of Te concentration on impurity segregation at complex defects.

I. INTRODUCTION

The distribution of defects, impurities, and of several physical parameters is known to be inhomogeneous in III-V wafers, often showing W-, M-, or U-shaped profiles across a wafer diameter. In a previous work[1] cathodoluminescence (CL) of scanning electron microscopy (SEM) has been used to study the distribution and nature of defects in GaAs:Te wafers with different Te concentrations. Profiles of near-band-edge CL intensity showed a U shape and profiles of infrared CL intensity had an inverted U shape. The appearance of defects in CL images was found to depend on doping level. In particular, in the samples with high Te content a fine background of unidentified dark defects was observed in addition to the typical dot and halo dislocation CL contrast. In order to get a more complete defect characterization and to correlate recombination centre distribution with minority-carrier diffusion length, further characterization techniques have to be applied. For this reason, in the present work the same sets of samples used in Ref. 1 have been studied by electron-beam-induced current (EBIC) in SEM and the diffusion length has been measured by surface photovoltage (SPV) technique.

II. EXPERIMENTAL PROCEDURE

A. Specimens

Wafers of liquid-encapsulated-Czochralski gallium arsenide Te doped, [100] oriented, have been studied. In order to investigate both the radial distribution of defects and impurities along the wafer diameter and the effects of doping on the formation of deep centers, three wafers, hereinafter denoted as A, B, and C, obtained from three different boules with average free carrier concentrations N_D-N_A equal to 2.2×10^{17} cm^{-3}, 4.5×10^{17} cm^{-3}, and 1.5×10^{18} cm^{-3}, respectively, have been studied. For each wafer the measurements have been carried out on 5-mm-wide strips cut along the wafer diameter, which, in turn, have been cut in ten parts so as to obtain 5×5 mm^2 samples (Fig. 1).

These samples, previously investigated by cathodoluminescence,[1] have been mounted on a single specimen holder for both charge collection scanning microscopy investigations and diffusion length measurements.

The Schottky barriers required by both the above said methods have been achieved by evaporating semitransparent (200 Å thick) Au dots on the samples. The ideality factor of the diodes so obtained has been determined to be close to 1 (1.03–1.07).

B. Methods

The distribution of the minority carrier diffusion length L across the wafers has been measured by the surface photovoltage (SPV) technique[2] with a SPEX spectrometer at room temperature. Low injection conditions were maintained during all the measurements, and the monochromator output slit was set as small as possible in the whole range of photon wavelengths explored in order to obtain the best spectral resolution. The spot size, determined by the dot diameter (1 mm) times the output slit width was $\leq5\times10^4$ μm^2.

The radial distribution of the net ionized shallow impurity concentration N_D-N_A has been obtained by capacitance-voltage measurements performed on the Schottky diodes prepared along the wafer diameter.

Electron beam induced current (EBIC) method has been used in order to correlate the radial distribution of the SPV diffusion length to the morphology and topological distribution of electrically active defects. Since efficient recombination centers, which strongly affect the minority-carrier diffusion length, can be associated with extended defects as well as to "pointlike" defects, the identification of the dark spots imaged by SEM/EBIC observations has been done in a way[3,4] which allows an unambiguous characterization of the defects at which recombination takes place, both in the

 0021-8979/94/76(2)/987/6/$6.00

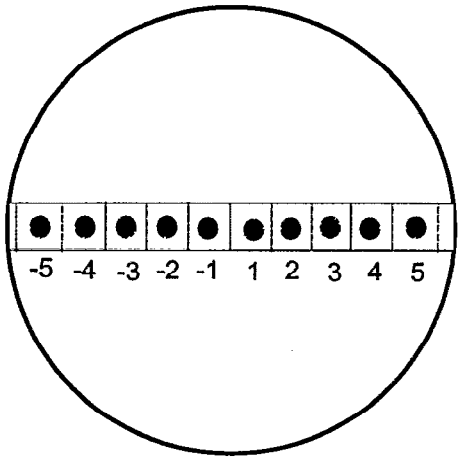

FIG. 1. Sketch of the distribution of the samples along the wafer diameter (50 mm).

space-charge region and in the bulk. Indeed, identification of the dark spots is necessary to distinguish between dislocations emerging at the sample surface and aggregates located in the bulk of the semiconductor. This identification has been made possible by using the SEM/EBIC method suggested by Sieber[3] for III-V compounds. The contrast curve as a function of the maximum electron range R (or, equivalently, of the beam voltage V_b) of an electrically active dislocation is M-shaped, while the contrast curve of a "less-active" dislocation and of a "pointlike" defect exhibits only one maximum.

The energy-dependent EBIC method of Wu and Wittry[5] has been used in order to locally determine minority-carrier diffusion length L and net ionized shallow impurity concentration N_D-N_A at and in the close proximity of defects.

III. RESULTS

The EBIC micrographs of sets A, B, and C (Fig. 2) show significant differences in the recombining center features depending on the doping level. Small (<1 μm) and medium (2 μm) size dots have been observed in wafer A [Fig. 2(a)], which exhibit a contrast c ranging from 5% to 15%, with $c=(1-I_d/I_0)$ where I_d and I_0 are the collected signal at the defect and far away from the defect, respectively. By applying the above said method[3,4] for the identification of the dark spot nature, EBIC contrast measurements versus beam voltage V_b have been carried out. Most dark spots were identified as dislocations since the contrast profiles showed two well-separated maxima (Fig. 3).

No bright halos are visible around the dots unless the beam voltage V_b is smaller than 10 kV, corresponding to a maximum electron range R_e equal to 0.49 μm.[6] Below this voltage the resolution improves sufficiently to show fine and weak bright regions around some of the dots. A few of the dots appear to be connected by thin dark contrast lines (k, l, and m pairs in Fig. 4), which suggests that they are grown-in and then stress-induced glide dislocations.[7] The background is uniform and bright. A similar dot and halo contrast, associated with the presence of dislocations, was observed in the near-band-edge cathodoluminescence images of the same samples.[8]

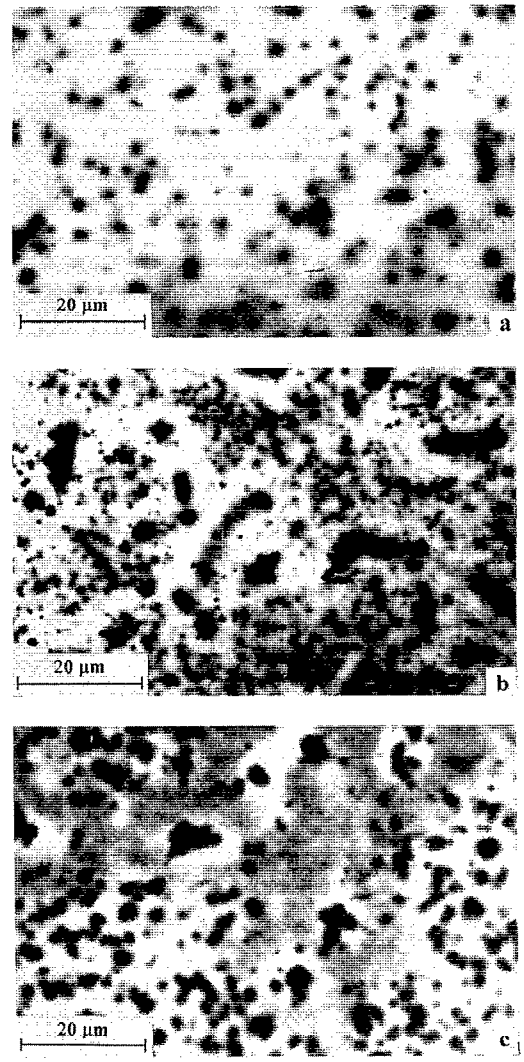

FIG. 2. EBIC images of samples from the set, A, B, and C, in (a), (b), and (c), respectively. The beam accelerating voltage was 20 keV.

In wafer B [Fig. 2(b)] the dot size ranges between 1 and 4 μm, the largest ones being surrounded by marked bright halos about 10 μm wide, and their contrast reaches up to 50%. The background is full of smaller dots and is highly inhomogeneous.

The samples obtained from both the slices B and C exhibit a background with a nonuniform recombination activity, which is impossible to resolve. In these specimens, in addition, the presence of "agglomerates" [Figs. 2(b) and 2(c)] occurs; however, a marked difference of the samples from the wafer C in respect to those from the wafer B can be observed: the agglomerates from the former wafer, only, are surrounded by regions 40–50 μm wide, devoid of dots. These agglomerates, outlined by thin, bright halos [Fig. 5(a)] which disappear when the sample is directly biased [Fig. 5(b)], consist of several small recombining dots as revealed

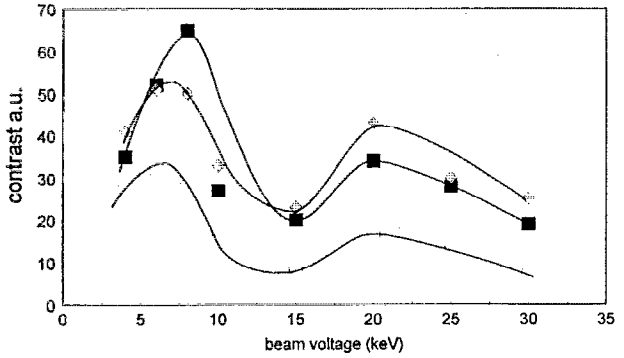

FIG. 3. Some examples of dislocation EBIC contrast c as a function of the beam accelerating voltage V_b. These results refer to measurements performed in samples from the wafer A.

by conveniently improving the resolution under direct bias conditions [Fig. 5(b)].

From the dot and halo CL images of the same samples, the dislocation density profile along the wafer diameter, shown in Fig. 6, has been obtained.

The radial distribution of the net ionized shallow impurity density N_D-N_A deduced by capacitance-voltage (C-V) measurements is reported in Fig. 7. The concentration N_D-N_A of the net ionized shallow impurities is inhomogeneous and its profile is M-shaped. It is worth noting that the inhomogeneity of N_D-N_A across the wafer diameter increases with the doping level, so that the difference between the maximum value $(N_D-N_A)_M$ and the minimum one $(N_D-N_A)_m$ (usually found at the wafer center), normalized to the latter value, is $[(N_D-N_A)_M-(N_D-N_A)_m]/(N_D-N_A)_m = 1.1$ for the wafer A, 2.1 for the wafer B, and 12 for wafer C.

The EBIC energy-dependent method for the localized evaluation of the minority-carrier diffusion length L and the space-charge region (SCR) width w made it possible to determine the local ionized carrier concentration N_D-N_A,[5,9] with a spatial resolution on the order of 1 μm. In these measurements, carried out on dots, bright halos, and matrix, N_D-N_A has been deduced by means of the formula[10]

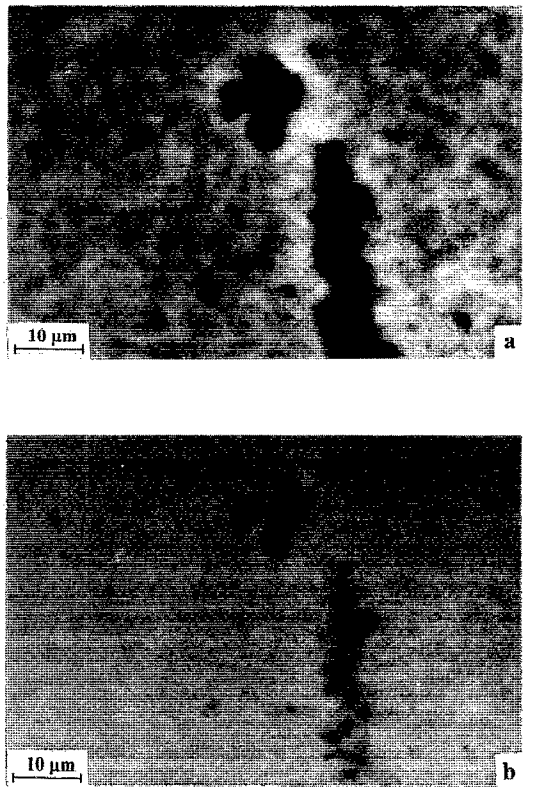

FIG. 5. EBIC micrograph of an "agglomerate" (a) without applied bias and (b) under direct bias conditions (bias voltage=0.7 V, beam accelerating voltage V_b=10 kV).

$$N_D-N_A=2\epsilon\epsilon_0 V_0/(qw^2), \tag{1}$$

where ϵ and ϵ_0 are the relative and absolute dielectric constant, respectively, V_0 the built-in potential of the diode, and q the electronic charge. This equation, valid when the deep-level density N_T is negligible in comparison to the free-carrier concentration, has been used here, assuming that the above condition holds in all of the wafers examined, due to their high doping concentration, and thus even inside the dots also in the case of deep level generation.

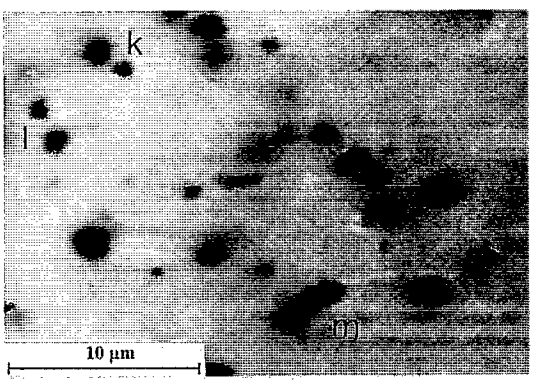

FIG. 4. Micrograph of dots in wafer A. Grown-in defects are labelled k, l, and m.

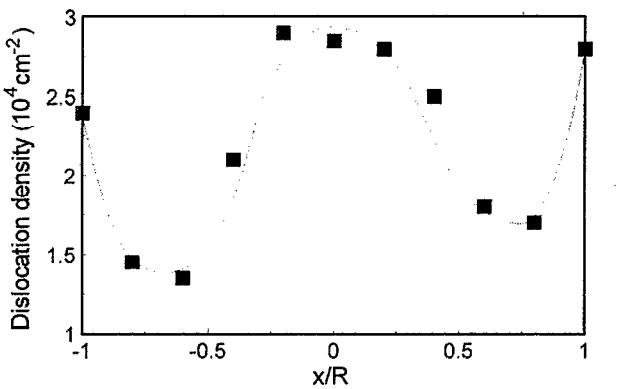

FIG. 6. Dislocation density across the diameter in the GaAs:Te-doped wafer A.

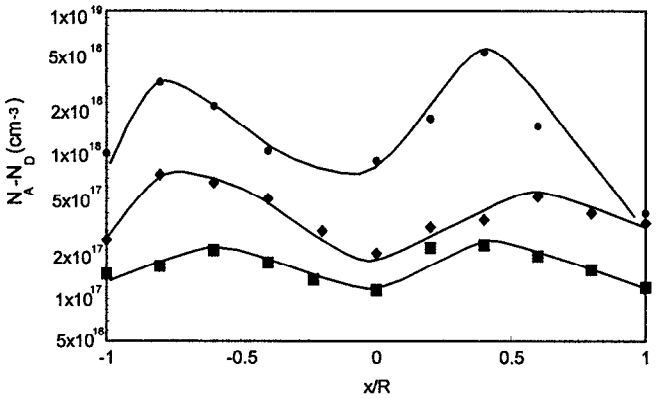

FIG. 7. Profiles of the ionized shallow impurity concentration N_D-N_A across the diameter of the sets A (■), B (♦), and C (●). x is the distance from the wafer center, R is the wafer radius.

The local free-carrier concentration significantly depends on the electron-beam position, Fig. 8(a), varying from the maximum value in the bulk to a minimum in the halo and to an intermediate value in the dot. This behavior, enhanced

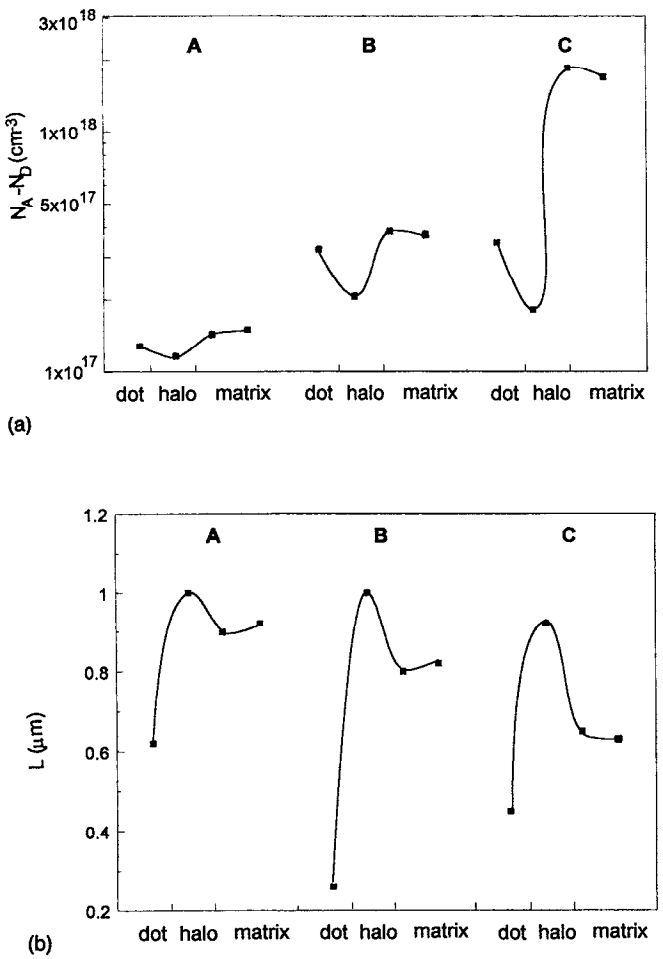

FIG. 8. (a) Free-carrier concentration and (b) diffusion length in dot, halo, and matrix regions of wafers A, B, and C.

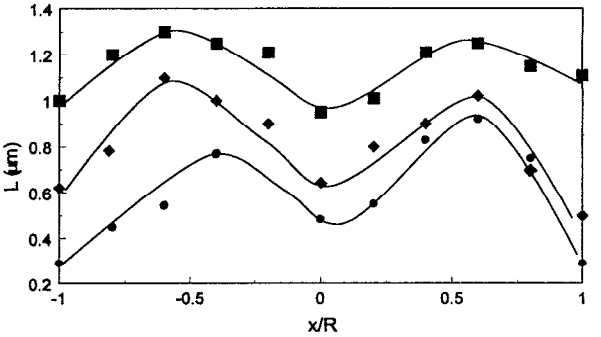

FIG. 9. Radial distribution of SPV diffusion length across wafer A (■), B (♦), and C (●). x is the distance from the wafer center, R is the wafer radius.

by increasing the doping level, suggests that the impurity segregation at the extended defects depends on the doping concentration.

The SPV diffusion length L distribution across the wafer diameter exhibits the same M-shaped behavior (Fig. 9) as the net ionized shallow centre density. As for the N_D-N_A distribution, the L inhomogeneity also increases when the doping level increases.

The EBIC local results on L [Fig. 8(b)] differ from what is expected from the N_D-N_A local behavior. The determination of L in dots, bright halos, and matrix showed that the minority-carrier diffusion length has the highest value in the halos and the lowest one in the dots. From these localized measurements it stems that L is mostly affected by nonradiative recombination at deep centers at the dots, rather than by radiative recombination depending on the net ionized shallow impurities. If the diffusion length changes were controlled by band-to-band radiative recombination, L would have much higher values, ranging, for example, in wafer A, from 7.5 μm in the halo to 4.4 μm in the dot, as determined from the dopant concentration as follows:

$$L=(D/Bn)^{1/2}, \tag{2}$$

with D the diffusion constant, n the majority-carrier concentration ($\approx N_D-N_A$), and B a constant that for GaAs is 1.7×10^{-10} cm^3/s.[11]

IV. DISCUSSION

The EBIC micrographs of Fig. 2 show that different kinds of electrically active defects are present in the investigated wafers: large (about 10 μm) and small (~1–2 μm) dots surrounded by a halo and a fine distribution of smaller dots without halo. The latter kind of defects is observed only in wafers B and C, which have higher values of Te concentrations.

The beam energy dependence of EBIC contrast (Fig. 3) shows that the large and medium size dots are dislocations as demonstrated when the procedure of Ref. 3 is considered. Usually the corresponding CL images do not enable the ready identification of the medium size dots as dislocations. The dislocation character of the smallest dots cannot be investigated by the EBIC contrast due to their size; however,

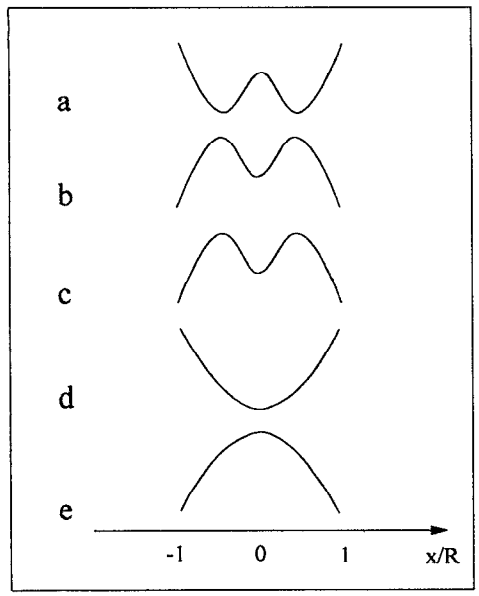

FIG. 10. Schematic diagrams of the distribution across the wafer of (a) dislocation density, (b) majority-carrier density N_D-N_A, (c) diffusion length L, (d) near-band-edge CL, and (e) infrared CL.

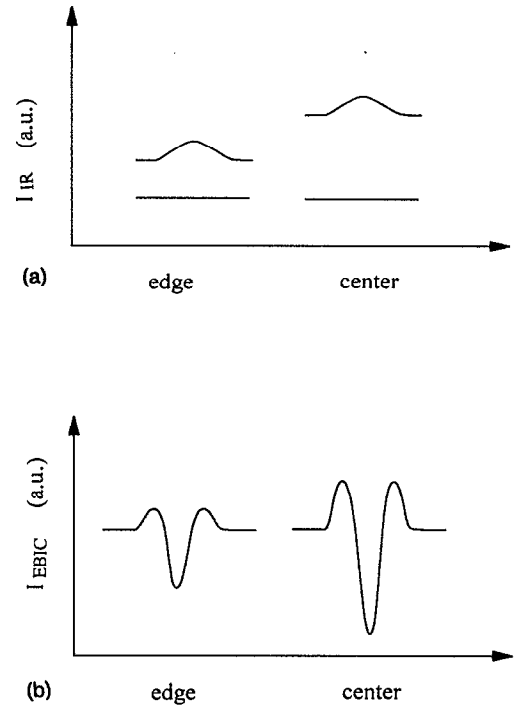

FIG. 11. (a) Dislocation infrared CL emission profiles at the wafer edge (on the left-hand side) and at the center (on the right-hand side), and (b) EBIC dislocation profiles at the corresponding locations. In (a) the horizontal line represents the reference (zero) level of the emission intensity.

the fact that some new dots appear in the EBIC image by increasing beam energy indicates that they are nonextended microdefects[12] rather than dislocations. In the following the results relevant to dislocation related dots are discussed.

Previous works[1,8] indicate that impurity-point defect complexes such as Te_{As}-V_{Ga} are involved in the luminescence around dislocations in GaAs:Te, although the existence of other larger complexes such as Te_{As}-V_{Ga}-V_{As} has been also considered.[13] In particular the Te_{As}-V_{Ga} complex has been related to an infrared emission band at 1.2–1.3 eV. Spatially resolved CL observations[1] have shown that this emission is mainly localized at the points where the dislocations intersect the surface, giving rise to a CL contrast opposite to that obtained with near-band-edge emission. This indicates that the complex concentration is higher at dislocation centers than in the bulk. The present results enable further characterization of point defects at and around dislocations.

As shown in Fig. 8 the free-carrier concentration is markedly higher in the dot than in the halo and both values are lower than in the bulk. The gettering of Te by the dislocations explains the low value in the halo since it must be expected that the impurities leave the bright halo region around the dislocations giving rise to an area depleted of shallow active impurities. The bulk value, higher than the dot, could be due to the conversion of Te into an electrically inactive state by forming complexes, such as Te_{As}-V_{Ga}, at the dislocations. This hypothesis also explains the L trend, controlled by recombination at deep centers. This possibility agrees with the above-mentioned observations of CL infrared emission at dislocations. Part of these observations can be correlated with the radial distribution of defects and defect related properties sketched in Fig. 10.

In this respect it is worth noting that, since the doping levels in the three wafers investigated vary significantly from center to edge so that the same doping level is found at different positions on the different wafers (compare, for example, in Fig. 7 the value of N_D-N_A at $x/R=0$ in the wafer B to the value at $x/R=0.5$ in the wafer A), the same characteristic EBIC images are found in areas from different wafers but with the same doping level. Referring to the above example, in the specimens from the slice A the dark dots exhibit a bright halo in diodes from areas close to $x/R=0.5$, while the halo vanishes when the doping level decreases going toward the center or to the edges of the wafer.

In addition to the results of this work the visible and near-infrared CL profiles previously observed in the same samples are included in Fig. 10. The dislocation density profile across the wafer [curve (a)] is inverse to the free carrier concentration profile [curve (b)] due to the gettering of Te by dislocations which reduces the density of electrically active states. The M-shaped distribution of the diffusion length L (c) shows that the controlling factor of this parameter is not the free-carrier density but the dislocations and their associated atmosphere of point defects and complexes. This interpretation agrees with the near-band-edge CL profile [curve (d)] found in the same set of samples. Curve (d) has been explained[1] by gettering of nonradiative centers, probably vacancies at dislocations. High CL emission in curve (d) corresponds to a low vacancy concentration possibly due to the formation of tellurium-vacancy complexes.

In order to correlate the present results with the infrared CL profile [curve (e)] the particular features of this emission

have to be considered. Besides the dislocation-related infrared emission there is an inhomogeneous distribution, not dislocation dependent, of infrared centers across the wafer.[14] In Ref. 14 it was found that in the wafer center there is an infrared background emission higher than in the wafer edge. A difference has also been observed in the EBIC profile across dislocations, even though it does not significantly affect the EBIC results. Consequently the emission at the dislocations in both regions can be sketched as in Fig. 11. For this reason the infrared CL and dislocation density profiles are inverse although dislocations appear bright in the infrared images. This suggests that dislocation-related centers, and not the centers responsible for the mentioned background emission, determine the L values measured across the wafer.

ACKNOWLEDGMENTS

This work was supported by the Comisíon Interministerial de Ciencia y Tecnología (Project No. PB90-1017) and by the Italian MURST. The authors wish to thank Wacker-Chemitronic (Dr. K. Löhnert) for providing the samples.

[1] B. Mendez and J. Piqueras, J. Appl. Phys. **69**, 2776 (1991).
[2] A. M. Goodman, J. Appl. Phys. **53**, 7561 (1982).
[3] B. Sieber, Phil. Mag. B **55**, 585 (1987).
[4] B. Sieber, Izvest. Acad. Nauk USSR Ser. Fiz. **51**, 650 (1987).
[5] C. J. Wu and D. B. Wittry, J. Appl. Phys. **49**, 2827 (1978).
[6] J. Orton and P. Blood, *The Electrical Characterization of Semiconductors: Measurements of Minority Carrier Properties* (Academic, New York, 1990).
[7] C. Frigeri and J. L. Weyher, J. Appl. Phys. **65**, 4646 (1989).
[8] B. Mendez, J. Piqueras, F. Domínguez-Adame, and N. de Diego, J. Appl. Phys. **64**, 4466 (1988).
[9] C. Frigeri and O. Breitenstein, in *Defect Control in Semiconductors*, edited by K. Sumino (Elsevier, Amsterdam, 1990), p. 685.
[10] S. Sze, *Physics of Semiconductor Devices* (Wiley, New York, 1981).
[11] R. D. Ryan and J. S. Eberhart, Solid-State Electron. **15**, 862 (1972).
[12] A. Govorkov and L. Kolesnik, Sov. Phys. Semicond. **12**, 259 (1978).
[13] B. Hughes and G. H. Narayanan, Phys. Status Solidi A **46**, 627 (1978).
[14] B. Mendez, Ph.D. thesis, Universidad Complutense, Madrid, Spain, 1991.